ELECTRONIC SUPPLEMENTARY INFORMATION

Optical trapping and optical force positioning of two-dimensional materials

M. G. Donato,[*a] E. Messina,[a‡] A. Foti,[a] T. Smart,[b] P. H. Jones,[b] M. A. Iatì,[a] R. Saija,[c] P. G. Gucciardi,[a] and O. M. Maragò[*a]

S1 Optical characterization of exfoliated samples

UV-Vis absorption spectroscopy. The hBN, MoS_2 and WS_2 aqueous dispersions reported in the main text have been studied with UV-Vis absorption spectroscopy, by means of a Perkin Elmer Lambda 25 UV-Vis spectrometer. In Fig. S1(a), the measured extinction spectra are shown. The agreement with literature results[9,20] can be easily verified.

Raman spectra of drop-casted hBN flakes. Aiming at verifying the effectiveness of the exfoliation process of hBN, a systematic Raman study on samples obtained by drop-casting the hBN dispersion on a SiO_2/Si substrate has been carried out. The results are summarized in Fig. S1(b). We found that Raman spectroscopy is consistent with the presence of mono- and few-layer flakes in solution[10], even if in measurements on drop-cast samples the highest blue shift (~ 2 cm^{-1}) is lower than the value (~ 4 cm^{-1}) found in the trapping measurements. This could be due to some flake re-aggregation induced by the drop-casting process.

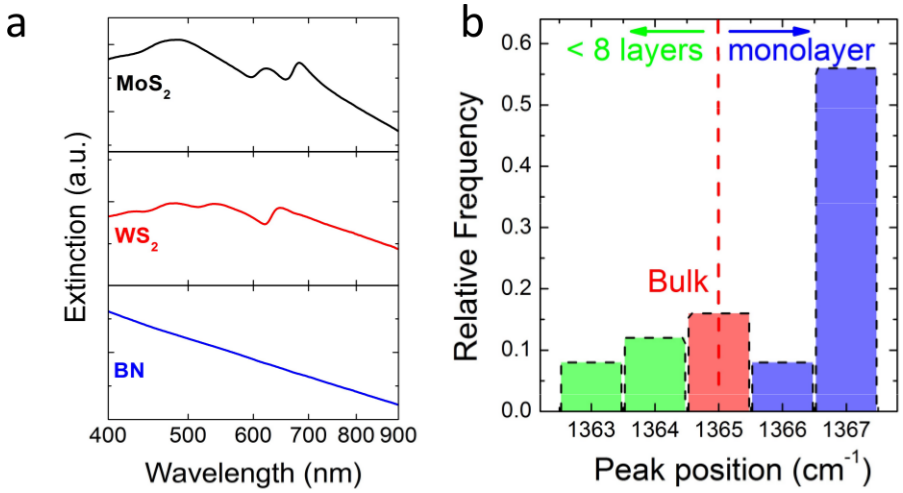

Figure 1: *

Figure S1: (a) UV-Vis absorption spectra of 2D materials studied in the main text. (b) Raman characterization of hBN flakes drop-casted on a Si substrate. Exciting wavelength 633 nm.

[0a] *CNR-IPCF, Istituto per i Processi Chimico-Fisici, V.le F. Stagno D'Alcontres 37, I-98158, Messina, Italy. Fax: 39 090 3974130; Tel: 39 090 39762249; E-mail: donato@ipcf.cnr.it, onofrio.marago@cnr.it*

[0b] *Department of Physics and Astronomy, University College London, London WC1E 6BT, UK.*

[0c] *Dipartimento di Scienze Matematiche e Informatiche, Scienze Fisiche e Scienze della Terra, Università di Messina, V.le F. Stagno D'Alcontres 31, I-98166, Messina, Italy.*

[0‡] Current address: CNR-ISMN, Istituto per lo studio dei materiali nanostrutturati, Via Salaria Km 29300, 00015, Monterotondo Stazione, Roma, Italy.

S2 Optical trapping and metrology of boron nitride

Optical trapping. In optical tweezers, optical forces on the trapped particle due to the interaction with the laser beam can be estimated by studying the Brownian motion of the particle in the confining optical potential. The corresponding Langevin equation is[12]:

$$m\frac{d^2}{dt^2}\mathbf{r}(t) = -\nabla U(\mathbf{r}) - \gamma\frac{d}{dt}\mathbf{r}(t) + \chi(t) \tag{1}$$

where $U(r)$ is the effective confining potential, γ is the friction coefficient and $\chi(t)$ is a random force with the properties of a white noise, *i.e.*, $\langle\chi(t)\rangle = 0$ and $\langle\chi(t)\chi(t+\tau)\rangle = 2\gamma k_B T$, with k_B the Boltzmann constant and T the absolute temperature. In this equation, the particle diffusion, governed by the term $\gamma\frac{d}{dt}r(t)$, is limited by the confining potential. In the over-damped regime, *i.e.*, when the friction is dominant on inertia[12], the term on the left of the eq. 1 can be neglected, leaving the overdamped Langevin equation:

$$\frac{d}{dt}\mathbf{r}(t) = -\frac{1}{\gamma}\nabla U(\mathbf{r}) + \xi(t) \tag{2}$$

where $\xi(t) = \chi(t)/\gamma$. In the case of small displacements of the particle in the trap, the confining potential can be considered as harmonic.

In this work, we model our trapped hBN particles as extremely thin disks (of diameter d) parallel to the xz plane (x beam polarization, z beam propagation). In this case, we have to consider the translational drag coefficient $\gamma_\perp = \frac{16}{3}\eta d$ for particle displacements in the x and z directions (displacements perpendicular to the symmetry axis of the flake), and the drag coefficient $\gamma_\parallel = 8\eta d$ for displacements in the y direction[13].

The 3D overdamped Langevin equation for a flat spheroidal particle becomes:

$$\frac{dx}{dt} = -\frac{k_x}{\gamma_\perp}x(t) + \xi_x(t) \tag{3}$$

$$\frac{dy}{dt} = -\frac{k_y}{\gamma_\parallel}y(t) + \xi_y(t) \tag{4}$$

$$\frac{dz}{dt} = -\frac{k_z}{\gamma_\perp}z(t) + \xi_z(t) \tag{5}$$

where k_x, k_y and k_z are the trap spring constants in the x, y and z directions, z being the beam propagation direction.

The main goal of optical trapping experiments is to recover, from the tracking of the particle fluctuations in the trap, the trap spring constants k_i and the conversion factors β_i between experimental units of the tracking signal (volts) and physical distance (μm). Various techniques can be used[12]; here, we will discuss the method of the particle position autocorrelation functions (ACFs) and, for the sake of simplicity, we will specify the analysis for one direction, x.

The particle position autocorrelation function C_{xx} in the x direction is:

$$C_{xx}(\tau) = \langle x(t)x(t+\tau)\rangle \tag{6}$$

By using the overdamped Langevin equation, we find that

$$C_{xx}(\tau) = \langle x(t)x(t+\tau)\rangle = C_{xx}(0)e^{-\omega_x\tau} = \frac{k_B T}{k_x}e^{-\omega_x\tau} \tag{7}$$

where

$$\omega_x = \frac{k_x}{\gamma_\perp} \tag{8}$$

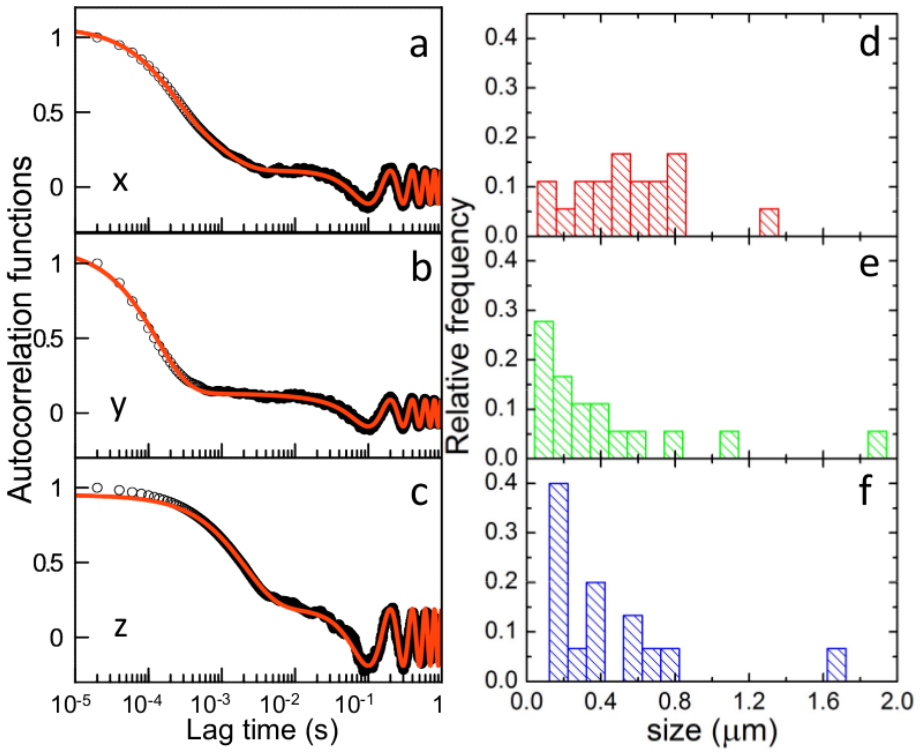

Figure 2: *

Figure S2: (a-c) Signal autocorrelation functions obtained by setting a 5 Hz sinusoidal oscillation along the x, y and z directions. (d-f) Measurements of the hBN flake diameter obtained by using the drag force method as explained in the main text. The mean flake size obtained by averaging all the measurements is shown in Fig. 2d of the main text.

is the ACF relaxation frequency and the amplitude of the last term can be obtained by the equipartition theorem[12]. Thus, by fitting the ACF with a single exponential decay, we may calculate the trap spring constant. However, the detector used to track the particle displacements records voltage signals $V_x(t) = \beta_x x(t)$, and, thus, we have to calibrate the trap in order to find the voltage/length conversion factor β_x

$$C^V_{xx}(\tau) = \beta_x^2 C_{xx}(\tau) = \beta_x^2 \frac{k_B T}{k_x} e^{-\omega_x \tau} \tag{9}$$

Thus, from the fit of the voltage autocorrelation function we obtain both the trap spring constant k_x and the voltage/length conversion factor β_x provided the knowledge of the corresponding damping coefficient. In the case of a spherical particle in 3D, all the formalism can be generalized to obtain the trap spring constants k_i and the corresponding conversion factors, provided that the drag coefficient is known. In the case of a non-spherical particle, a modelization of the particle shape must be used, in which different drag coefficients for translations in direction parallel and perpendicular to the particle symmetry axis, $\gamma_\perp$ and $\gamma_\parallel$, and for rotations, are considered. This has been already shown for 1D particles such as carbon nanotubes[14] or 2D graphene flakes[13] or even plasmonic silver nanoplatelets[15]. Also in these cases, the particle relevant size parameters (tube length or flake diameter) are generally measured independently and used to estimate the drag coefficients.

Flake metrology. As outlined above, the measurements of the trap force constants and the reconstruction of the Brownian motion generally require the knowledge of the size and shape of the trapped particle. If the particle size is not known, Eqs. 8 and 9 alone are not enough to calibrate the trap, and a third equation for the drag coefficients of the particle is needed. To this aim, we can use the method of the drag force, outlined in refs.[8,21].

We used a nanopositioning system (Mad City Labs Nano-LP200) giving a controlled sinusoidal oscillation to the microscope stage

$$x(t) = A_{stage}\sin(\omega_{stage}t) \tag{10}$$

where A_{stage} is the oscillation amplitude and ω_{stage} is the oscillation angular frequency. In this case, the fluid velocity is

$$v_{fluid} = v_{stage} = A_{stage}\omega_{stage}\cos(\omega_{stage}t) \tag{11}$$

and a trapped particle is subjected to a drag force

$$F_{drag} = -\gamma_{\perp}v_{stage} = -\gamma_{\perp}\omega_{stage}A_{stage}\cos(\omega_{stage}t) \tag{12}$$

When the fluid velocity is lower than the escape velocity of the particle from the trap, the optical restoring force k_x is in equilibrium with the maximum drag force and then

$$k_x a_V = \beta_x \gamma_{\perp}\omega_{stage}A_{stage} \tag{13}$$

where β_x is the same voltage/length calibration factor seen in eq. 9 and a_V is the detector voltage signal corresponding to the particle displacement in the trap.

If a trapped particle is subjected to an oscillation, its displacement can be written as[11]

$$S_x(t) = x_V(t) + a_V\sin(\omega_{stage}t) \tag{14}$$

Its autocorrelation function can be fitted with the sum of one (or two, if the particle is not spherical, to take into account rotational fluctuations[11,13]) exponential decay and a cosinusoidal modulation[11]

$$C^V_{xx}(\tau) = Ae^{-\omega_x\tau} + \frac{a_V^2}{2}\cos(\omega_{stage}\tau) = \beta_x^2\frac{k_BT}{k_x}e^{-\omega_x\tau} + \frac{a_V^2}{2}\cos(\omega_{stage}\tau) \tag{15}$$

Thus, from the fit of the particle ACF, and in particular, from the value of the amplitude of the cosinusoidal modulation, we can calculate the quantity to be put in eq. 13. Thus, we have the absolute calibration of the trap, because, comparing eqs. 8 and 13, we obtain

$$\beta_x = \frac{\omega_x a_V}{\omega_{stage}A_{stage}}\ . \tag{16}$$

From the fit of the ACF, we obtain A and, thus,

$$k_x = \beta_x^2\frac{k_BT}{A}\ . \tag{17}$$

Finally, from the fit we obtain also ω_x and, thus, $\gamma_{\perp} = k_x/\omega_x$ and the particle size, d. Thus, once we obtain the drag coefficients, the flake lateral size, d, can be estimated for each measurement. In Fig. S2(a-c) some typical ACFs obtained on a trapped flake along the three spatial directions are shown, together with the (Fig. S2(d-f)) estimate of the flake lateral size d obtained for each direction by trapping several flakes. The mean flake size obtained by averaging on all the measurements is shown in Fig. 2d of the main text.

S3 Calculation of optical forces in the dipole approximation

To understand the different trapping/pushing behaviour observed in our exfoliated samples, we calculated optical forces in the dipole approximation[12]. The following calculations are based on two approximations: i) we consider particles that are sufficiently smaller than the trapping wavelength; ii) we consider an effective Gaussian beam with a waist matched to the diffraction limited spot. While both conditions can have some limitations in our experiments, these calculations provide a simple and easy way to show the different optomechanical response for the different material flakes.

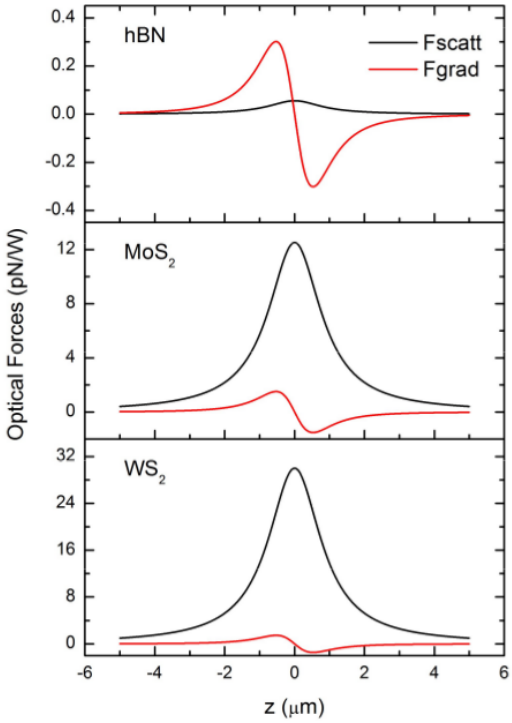

Figure 3: *

Figure S3: Scattering force (black curve) and gradient force (red curve) calculated in the direction of the beam propagation for the 2D materials studied in this work. In hBN F_{grad} is always greater than F_{scatt}, allowing the particle trapping. Data have been normalized for the laser power. Excitation wavelength 785 nm.

The radiation force due to a Gaussian beam of power P and waist w_0, propagating in the z direction, on a particle having size much smaller than the radiation wavelength and immersed in a medium with refractive index n_m, is:

$$\vec{F}_{rad} = \frac{n_m}{2}\frac{\mathrm{Re}\{\alpha\}}{c\varepsilon_m}\vec{\nabla}I + \frac{n_m\sigma_{ext}}{c}I\hat{z} \tag{18}$$

where $\mathrm{Re}\{\alpha\}$ is the real part of the particle polarizability, σ_{ext} the extinction cross section, c the speed of light and $I = \frac{2P}{\pi w_0^2}$ the incident light intensity in the medium. The first term in the right hand side of Equation 18 gives the gradient force F_{grad}, that confines the particle in the focal spot if the particle refractive index is higher than that of the medium[12]. The second term is the scattering force F_{scatt}, that pushes the particle along the beam propagation. Optical trapping occurs when gradient forces are larger than scattering forces.

Our flakes are modeled as oblate spheroids with 100 nm diameter and 6 nm thickness. As such, the modified Clausius-Mossotti expression in the static limit for the particle polarizability[3] is given by:

$$\alpha_i = V\varepsilon_m\left(\frac{\varepsilon_m}{\varepsilon_p - \varepsilon_m} + L_i\right)^{-1} \tag{19}$$

with V the spheroid volume, ε_p its complex permittivity, and L_i the spheroid geometrical factors with respect the principal axes $i = 1,2,3$. The choice of which geometrical factor to use in the calculation of the polarizability and, thus, the optical forces, depends on the alignment of the particle with respect the field polarization. In our calculation, we have considered that the particle long axes a_1 and a_2 are directed with the field polarization x and the beam propagation z, respectively. In this case, the gradient force along the z direction, considering $I(z) = \frac{I}{1+\frac{z^2}{z_R^2}}$ will be:

$$F_{grad} = -\frac{n_m \alpha_2 I}{c\varepsilon_m} \frac{z}{z_R^2} \left(1 + \frac{z^2}{z_R^2}\right)^{-2} \tag{20}$$

where $z_R = \frac{n_m \pi w_0^2}{\lambda}$ is the Rayleigh range. For the evaluation of the waist, we used $w_0 \sim 1.5 \cdot 0.61 \frac{\lambda}{NA\ n_m}$, with λ the excitation wavelength in vacuum, $0.61 \frac{\lambda}{NA\ n_m}$ the Abbe criterion for the focal spot radius in the diffraction limit. The prefactor 1.5 is introduced to take in account the polarization asimmetry of the focal spot[17].

To evaluate the scattering force, we need to calculate the extinction cross section σ_{ext} as a sum of scattering and absorption terms[12]:

$$\sigma_{ext} = \frac{k^4}{6\pi\varepsilon_0^2}|\alpha|^2 + \frac{k}{\varepsilon_0}\mathrm{Im}\{\alpha\} \tag{21}$$

where $k = \frac{2\pi n_m}{\lambda}$ is the wavevector.

The material permittivity ε_p has been calculated at three different wavelengths (638 nm, 785 nm and 830 nm) by referring to published results regarding the real (n) and imaginary (κ) parts of the 2D material refractive indexes[1,10,22]. We have found that in hBN, F_{grad} is greater the F_{scatt} at each wavelength considered, allowing the particle trapping. On the contrary, in MoS_2 and WS_2, F_{scatt} is always greater than F_{grad}, hindering the trapping. In Fig. S3, the comparison between F_{grad} and F_{scatt} is shown at 785 nm exciting wavelength.

S4 Optical forces in the T-matrix formalism for non-spherical particles

Optical forces and torques are calculated by solving the light scattering problem in the T-matrix approach[4,19]. We model our layered material flakes as planar cluster particles illuminated by the optical tweezers tightly focused beam (objective lens with NA=1.3). First, the focal optical fields of the optical tweezers are calculated in the absence of any particle by means of the angular spectrum representation in the original formulation by Richards and Wolf[6,16–18]. These focal field components are the incident fields to be used in the T-matrix formulation of the scattering problem. Thus, the radiation force and torque exerted on a particle within the focal region is obtained by integrating the time-averaged Maxwell stress tensor[6,12]:

$$\mathbf{F}_{\mathrm{rad}} = r^2 \oint_\Omega \overline{\mathsf{T}}_{\mathrm{M}} \cdot \hat{\mathbf{r}}\, d\Omega\,, \tag{22}$$

$$\mathbf{T}_{\mathrm{Rad}} = -r^3 \oint_\Omega \left(\overline{\mathsf{T}}_{\mathrm{M}} \times \hat{\mathbf{r}}\right) \cdot \hat{\mathbf{r}}\, d\Omega\,, \tag{23}$$

where the integration is over 4π, r is the radius of a large sphere surrounding the particle, and $\overline{\mathsf{T}}_{\mathrm{M}}$ is the time-averaged Maxwell stress tensor in the Minkowski form in a homogeneous, linear, and nondispersive medium[12] (water in our specific case):

$$\overline{\mathsf{T}}_{\mathrm{M}} = \frac{1}{2}\varepsilon_{\mathrm{m}} \mathrm{Re}\left[\mathbf{E} \otimes \mathbf{E}^* + \frac{c^2}{n_{\mathrm{m}}^2}\mathbf{B} \otimes \mathbf{B}^* - \frac{1}{2}\left(|\mathbf{E}|^2 + \frac{c^2}{n_{\mathrm{m}}^2}|\mathbf{B}|^2\right)\mathsf{I}\right]\,, \tag{24}$$

where $\mathbf{E}$ and $\mathbf{B}$ are the phasors of the total fields, $\otimes$ indicates dyadic product, I is the dyadic unit, ε_{m} is the dielectric permittivity of the medium, and n_{m} is the refractive index of the medium. The total fields are the superposition of incident and scattered fields, $\mathbf{E} = \mathbf{E}_{\mathrm{i}} + \mathbf{E}_{\mathrm{s}}$ and $\mathbf{B} = \mathbf{B}_{\mathrm{i}} + \mathbf{B}_{\mathrm{s}}$. Hence the radiation force and torque are expressed as[5,6,12]:

$$\mathbf{F}_{\mathrm{rad}} = -\frac{1}{4}\varepsilon_{\mathrm{m}} r^2 \oint_\Omega \left[|\mathbf{E}_{\mathrm{s}}|^2 + \frac{c^2}{n_{\mathrm{m}}^2}|\mathbf{B}_{\mathrm{s}}|^2 + 2\mathrm{Re}\left\{\mathbf{E}_{\mathrm{i}} \cdot \mathbf{E}_{\mathrm{s}}^* + \frac{c^2}{n_{\mathrm{m}}^2}\mathbf{B}_{\mathrm{i}} \cdot \mathbf{B}_{\mathrm{s}}^*\right\}\right] \hat{\mathbf{r}}\, d\Omega\,. \tag{25}$$

$$\mathbf{T}_{\mathrm{Rad}} = -\frac{\varepsilon_{\mathrm{m}} r^3}{2}\mathrm{Re}\left\{\oint \left[(\hat{\mathbf{r}} \cdot \mathbf{E})(\mathbf{E}^* \times \hat{\mathbf{r}}) + \frac{c^2}{n_{\mathrm{m}}^2}(\hat{\mathbf{r}} \cdot \mathbf{B})(\mathbf{B}^* \times \hat{\mathbf{r}})\right] d\Omega\right\}\,. \tag{26}$$

We note that while for the case of the optical force we can use the far-field expression of the fields and scattering amplitude[6], the calculation of the optical torque is more complex since it must include longitudinal terms in order to have a non-vanishing result[5]. We then expand the incident and scattered fields in vector spherical harmonics regular at the origin, Bessel **J**-multipoles, and regular at infinity, Hankel **H**-multipoles, respectively. The amplitudes of the incident fields expansion, $W^{(p)}_{\mathrm{i},lm}$, are known through the calculation of the focal fields, while the amplitudes of the scattered fields expansion, $A^{(p')}_{\mathrm{s},l'm'}$, are related to the incident amplitudes through the elements of the T-matrix, $T^{(p'p)}_{l'm'lm}$:

$$A^{(p')}_{\mathrm{s},l'm'} = \sum_{plm} T^{(p'p)}_{l'm'lm}\, W^{(p)}_{\mathrm{i},lm}\,, \tag{27}$$

with the indices $p = 1,2$ indicating the parity of the multipoles, and the indices $l = 0,1,...$ and $m = -l,...,0,...,l$, related to their angular momentum. By imposing the field boundary conditions across the particle surface we obtain a linear system whose matrix can be inverted to obtain the elements of the T-matrix. The optical force and torque components are finally calculated by a projection of each vector onto each coordinate unit vector and calculating the corresponding numerical integral[5,6].

To model our layered material flakes we consider a planar cluster composed by N (homogeneous) spheres of radius a_α and refractive index n_α (corresponding to the complex refractive index of each layered material), with $\alpha = 1, ..., N$, surrounded by a medium (water) with refractive index n_m. The spheres are centered at $\mathbf{R}_\alpha$ with respect to the common origin **O**. The field scattered by the whole aggregate is the superposition of the fields scattered by each sphere[4,19], i.e.,

$$\mathbf{E}_\mathrm{s}(\mathbf{r}) = \sum_{\alpha=1}^{N} \sum_{plm} \mathscr{A}^{(p)}_{\mathrm{s},\alpha lm} \mathbf{H}^{(p)}_{lm}(n_\mathrm{m} k_0 r_\alpha, \hat{\mathbf{r}}_\alpha)\,, \tag{28}$$

where $\mathbf{r}_\alpha = r_\alpha \hat{\mathbf{r}}_\alpha = \mathbf{r} - \mathbf{R}_\alpha$, $\mathscr{A}^{(p)}_{\mathrm{s},\alpha lm}$ are the translated amplitudes and k_0 is the wavenumber in vacuum. The field inside the α-th sphere is expanded as

$$\mathbf{E}_{\mathrm{p},\alpha}(\mathbf{r}) = \sum_{plm} \mathscr{W}^{(p)}_{\mathrm{p},\alpha lm} \mathbf{J}^{(p)}_{lm}(n_\alpha k_0 r_\alpha, \hat{\mathbf{r}}_\alpha)\,, \tag{29}$$

so that it is regular everywhere inside the sphere. The scattered field is given by a linear combination of multipole fields that have different origins, whereas the incident field is given by a combination of multipole fields centered at the origin of the coordinates. Since we must impose the boundary conditions at the surface of each sub-unit sphere, we use the addition theorem[7,12] for multipole fields to express the incident and scattered field at the surface of the α-th sphere. Applying the boundary conditions, we get four equations for each α, l and m among which the elimination of the amplitudes of the internal fields yields as final result a system of linear non-homogeneous equations for the shifted incident and scattered amplitudes[19], $\mathscr{W}^{(p)}_{\mathrm{i},\alpha lm}$ and $\mathscr{A}^{(p)}_{\mathrm{s},\alpha lm}$. Thus, the addition theorem allows us to write the scattered field by the whole aggregate in terms of multipole fields with common origin at **O** through the application of the matrix that translates the origin of the **H**-multipole fields from $\mathbf{R}_{\alpha'}$ to the common origin of the coordinates at **O**.

We used this general cluster model to calculate the light scattering process, optical forces and torques for our layered material flakes modeled as planar dielectric clusters. We considered cluster of increasing lateral size, d, composed of spherical sub-units of 10 nm radius. Figure 3 in the main text shows the results for optical trapping efficiencies, Q_x, Q_y, and Q_z, for a flake with the same planar structure but optical properties of hBN, MoS_2, and WS_2.

We note that the solution of the light scattering problem for a cluster and the evaluation of its T-matrix is related with the inversion of a complex matrix that, in principle, has infinite elements. As typical in this situation, we truncate the multipole expansion to some finite multipole order l_T, which is chosen to ensure, at a reasonable computational effort, the numerical stability of the calculated observables (e.g., cross-sections,

optical forces, and optical torques). In practice, we check computationally for the existence of a minimum l-value, l_{M} such that when $l_{\mathrm{T}} > l_{\mathrm{M}}$ the observable quantities do not change within numerical accuracy. Thus, for a cluster of N spheres, a matrix of order $dim = 2Nl_{\mathrm{T}}(l_{\mathrm{T}}+2)$ needs to be inverted. The truncation order to be considered in the multipole expansion of a cluster depends not only on the individual particle size, but also on the geometrical packing in the aggregate. As a rule-of-thumb we can consider the smallest sphere of radius $R_{cluster}$ that includes the whole cluster with a corresponding size parameter $x_{cluster} = 2\pi R_{cluster}/\lambda$ and truncate the expansion at $l_{\mathrm{T}} > x_{cluster}$. However, we verified that all our results are convergent within 0.1%.

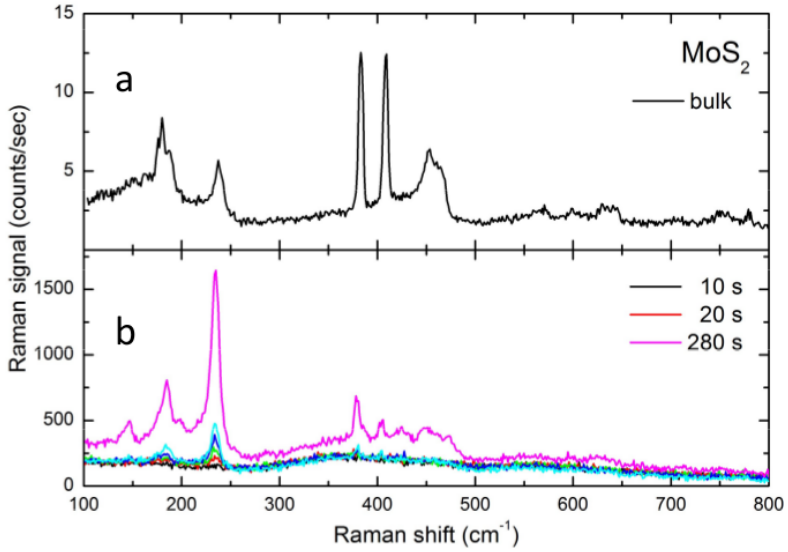

Figure 4: *

Figure S4: Raman spectra obtained on bulk MoS_2 (a) and under laser pushing of exfoliated MoS_2 at 785 nm (b). In (a), a long-working distance x50 objective (NA=0.5, laser power 0.6 mW) has been used, while in (b) a x100 oil immersion objective (NA=1.3, laser power 9.6 mW) has been used. In (b), a strong Raman peak at approximately 234 cm^{-1} can be associated to a longitudinal acoustic phonon that becomes Raman active due to presence of defects from the edges of the MoS_2 flakes.

S5 Raman spectroscopy of pushed MoS_2 at 785 nm

In the main text, the aggregation process of MoS_2 flakes under laser pushing at 638 nm is followed by studying the time evolution of the Raman spectrum. Here, a similar study is carried out under laser pushing at 785 nm (see Fig. S4). As it is sketched in the main text, in this spectrum, shown in Fig. S4(b), the most evident feature is a band at approximately 234 cm^{-1}, that is consistent with the presence of defects at the edge of our exfoliated flakes[2].

S6 Supplementary videos

The supplementary video 1 shows the 2D confinement of MoS_2 flakes when the laser beam is focused near the microscope slide (top) surface. In particular, we observe that the flakes are pushed towards the top surface and are trapped against the it, since the transverse gradient forces confine them in the laser spot. However, when the laser is off, the particles are free to move and disperse in the medium.

The supplementary video 2 shows that higher power, the flakes are temporarily stuck to the surface, but the aggregate is unstable. Furthermore, thermal effects such as the creation of bubbles in the host medium are observed, due to material absorption.

The supplementary video 3 shows the optical force positioning of MoS_2 flakes with BSA using a Laguerre-Gauss beam with $l = 30$. Orbiting of the flakes around the LG beam is observed at the beginning of the video due to the transfer of orbital angular momentum from the light to the flakes.

References

[1] S. Alfihed, M. Hossain, A. Alharbi, A. Alyamani, and F. H. Alharbi. PLD grown polycrystalline tungsten disulphide (WS2) films. *J. Mater.*, 2013:603648, 2013.

[2] É. Blanco, P. Afanasiev, G. Berhault, D. Uzio, and S. Loridant. Resonance raman spectroscopy as a probe of the crystallite size of MoS2 nanoparticles. *C. R. Chim.*, 19(10):1310–1314, 2016.

[3] C. F. Bohren and D. R. Huffman. *Absorption and scattering of light by small particles*. John Wiley & Sons, 1998.

[4] F. Borghese, P. Denti, and R. Saija. *Scattering from Model Nonspherical Particles*. Springer, Berlin, 2007.

[5] F. Borghese, P. Denti, R. Saija, and M. A. Iatì. Radiation torque on nonspherical particles in the transition matrix formalism. *Optics Express*, 14:9508–9521, 2006.

[6] F. Borghese, P. Denti, R. Saija, and M. A. Iatì. Optical trapping of nonspherical particles in the T-matrix formalism. *Opt. Express*, 15:11984–11998, 2007.

[7] F. Borghese, P. Denti, G. Toscano, and O. Sindoni. An addition theorem for vector helmholtz harmonics. *Journal of Mathematical Physics*, 21(12):2754–2755, 1980.

[8] A. Buosciolo, G. Pesce, and A. Sasso. New calibration method for position detector for simultaneous measurements of force constants and local viscosity in optical tweezers. *Opt. Commun.*, 230(4):357–368, 2004.

[9] J. N. Coleman, M. Lotya, A. O'Neill, S. D. Bergin, P. J. King, U. Khan, K. Young, A. Gaucher, S. De, R. J. Smith, et al. Two-dimensional nanosheets produced by liquid exfoliation of layered materials. *Science*, 331(6017):568–571, 2011.

[10] R. V. Gorbachev, I. Riaz, R. R. Nair, R. Jalil, L. Britnell, B. D. Belle, E. W. Hill, K. S. Novoselov, K. Watanabe, T. Taniguchi, et al. Hunting for monolayer boron nitride: optical and raman signatures. *Small*, 7(4):465–468, 2011.

[11] P. H. Jones, , F. Palmisano, F. Bonaccorso, P. G. Gucciardi, G. Calogero, A. C. Ferrari, and O. M. Maragó. Rotation detection in light-driven nanorotors. *ACS Nano*, 3(10):3077–3084, 2009.

[12] P. H. Jones, O. M. Maragò, and G. Volpe. *Optical tweezers: Principles and applications*. Cambridge University Press, Cambridge, 2015.

[13] O. M. Maragò, F. Bonaccorso, R. Saija, G. Privitera, P. G. Gucciardi, M. A. Iatì, G. Calogero, P. H. Jones, F. Borghese, P. Denti, V. Nicolosi, and A. C. Ferrari. Brownian motion of graphene. *ACS Nano*, 4:7515, 2010.

[14] O. M. Maragò, P. H. Jones, F. Bonaccorso, V. Scardaci, P. G. Gucciardi, A. G. Rozhin, and A. C. Ferrari. Femtonewton force sensing with optically trapped nanotubes. *Nano Lett.*, 8:3211–3216, 2008.

[15] E. Messina, M. G. Donato, M. Zimbone, R. Saija, M. A. Iatì, L. Calcagno, M. E. Fragala, G. Compagnini, C. D'Andrea, A. Foti, P. G. Gucciardi, and O. M. Maragò. Optical trapping of silver nanoplatelets. *Opt. Express*, 23(7):8720–8730, 2015.

[16] A. A. R. Neves, A. Fontes, L. d. Y. Pozzo, A. A. de Thomaz, E. Chillce, E. Rodriguez, L. C. Barbosa, and C. L. Cesar. Electromagnetic forces for an arbitrary optical trapping of a spherical dielectric. *Optics Express*, 14:13101–13106, 2006.

[17] L. Novotny and B. Hecht. *Principles of Nano-Optics*. Cambridge University Press, Cambridge, 2008.

[18] B. Richards and E. Wolf. Electromagnetic diffraction in optical systems. ii. structure of the image field in an aplanatic system. *Proc. R. Soc. A: Mathematical, Physical and Engineering Sciences*, 253:358–379, 1959.

[19] R. Saija, M. A. Iatì, F. Borghese, P. Denti, S. Aiello, and C. Cecchi-Pestellini. Beyond mie theory: the transition matrix approach in interstellar dust modeling. *The Astrophysical Journal*, 559(2):993–1004, 2001.

[20] R. J. Smith, P. J. King, M. Lotya, C. Wirtz, U. Khan, S. De, A. O'Neill, G. S. Duesberg, J. C. Grunlan, G. Moriarty, et al. Large-scale exfoliation of inorganic layered compounds in aqueous surfactant solutions. *Adv. Mater.*, 23(34):3944–3948, 2011.

[21] S. F. Tolić-Nørrelykke, E. Schäffer, J. Howard, F. S. Pavone, F. Jülicher, and H. Flyvbjerg. Calibration of optical tweezers with positional detection in the back focal plane. *Rev. Sci. Instrum.*, 77(10):103101, 2006.

[22] C. Yim, M. O'Brien, N. McEvoy, S. Winters, I. Mirza, J. G. Lunney, and G. S. Duesberg. Investigation of the optical properties of MoS2 thin films using spectroscopic ellipsometry. *Appl. Phys. Lett.*, 104(10):103114, 2014.